2013

Coupled Simulation of DNAPL Infiltration and Dissolution in Three-Dimensional Heterogeneous Domains: Process Model Validation

Amalia Kokkinaki
University of San Francisco, akokkinaki@usfca.edu

D M. O'Carroll

C J. Werth

B E. Sleep

Recommended Citation
Kokkinaki, A., D. M. O'Carroll, C. J. Werth, and B. E. Sleep (2013), Coupled simulation of DNAPL infiltration and dissolution in three-dimensional heterogeneous domains: Process model validation, Water Resour. Res., 49, 7023–7036, http://dx.doi.org/10.1002/wrcr.20503.

Coupled simulation of DNAPL infiltration and dissolution in three-dimensional heterogeneous domains: Process model validation

A. Kokkinaki,[1] D. M. O'Carroll,[2] C. J. Werth,[3] and B. E. Sleep[1]

Received 12 March 2013; revised 12 August 2013; accepted 24 August 2013; published 28 October 2013.

[1] A three-dimensional multiphase numerical model was used to simulate the infiltration and dissolution of a dense nonaqueous phase liquid (DNAPL) release in two experimental flow cells containing different heterogeneous and well-characterized permeability fields. DNAPL infiltration was modeled using Brooks-Corey-Burdine hysteretic constitutive relationships. DNAPL dissolution was simulated using a rate-limited mass transfer expression with a velocity-dependent mass transfer coefficient and a thermodynamically based calculation of DNAPL-water interfacial area. The model did not require calibration of any parameters. The model predictions were compared to experimental measurements of high-resolution DNAPL saturations and effluent concentrations. The predicted concentrations were in close agreement with measurements for both domains, indicating that important processes were effectively captured by the model. DNAPL saturations greatly influenced mass transfer rates through their effect on relative permeability and velocity. Areas with low DNAPL saturation were associated with low interfacial areas, which resulted in reduced mass transfer rates and nonequilibrium dissolution. This was captured by the thermodynamic interfacial area model, while a geometric model overestimated the interfacial areas and the overall mass transfer. This study presents the first validation of the thermodynamic dissolution model in three dimensions and for high aqueous phase velocities; such conditions are typical for remediation operations, especially in heterogeneous aquifers. The demonstrated ability to predict DNAPL dissolution, only requiring prior characterization of soil properties and DNAPL release conditions, represents a significant improvement compared to empirical dissolution models and provides an opportunity to delineate the relationship between source zone architecture and the remediation potential for complex DNAPL source zones.

Citation: Kokkinaki, A., D. M. O'Carroll, C. J. Werth, and B. E. Sleep (2013), Coupled simulation of DNAPL infiltration and dissolution in three-dimensional heterogeneous domains: Process model validation, *Water Resour. Res.*, *49*, 7023–7036, doi:10.1002/wrcr.20503.

1. Introduction

[2] Dense nonaqueous phase liquids (DNAPLs) present in the subsurface frequently persist as sources of long-term groundwater contamination. Even though DNAPL source zone remediation strategies have been the subject of extensive research to date, it remains a challenge to reliably predict the evolution of DNAPL source zones in the subsurface and the associated effect on downgradient effluent concentrations. Numerous studies have shown that source zone architecture has a strong impact on mass transfer from the DNAPL to the aqueous phase [*Christ et al*., 2006; *Fure et al*., 2006; *Lemke and Abriola*, 2006; *DiFilippo et al*., 2010]. As a result, uncertainties related to source zone spatial characteristics often hinder the accurate prediction of downstream concentrations. At the same time, the spatial evolution of the source zone itself is governed by the kinetics of mass transfer from the DNAPL to the aqueous phase (i.e., dissolution). Understanding the complex interplay between the DNAPL source zone architecture and the resulting effluent concentration is essential to addressing the problem of DNAPL source zone remediation.

[3] To date, the dissolution of DNAPLs has been studied under a wide variety of conditions, by both physical and numerical experiments and across most scales. It is well established that local equilibrium is often an invalid assumption, and that kinetic effects occur under most realistic conditions, when soil and source zone heterogeneity exist [*Unger et al*., 1998; *Maji and Sudicky*, 2008]. To capture these kinetic effects at the local, representative elementary volume (REV) scale, multiphase numerical

[1]Department of Civil Engineering, University of Toronto, Toronto, Ontario, Canada.
[2]Department of Civil and Environmental Engineering, University of Western Ontario, London, Ontario, Canada.
[3]Department of Civil and Environmental Engineering, University of Illinois at Urbana-Champaign, Urbana Illinois, USA.

Corresponding author: B. E. Sleep, Department of Civil Engineering, University of Toronto, 35 St. George St., Toronto, ON M5S 1A4, Canada. (sleep@ecf.utoronto.ca)

0043-1397/13/10.1002/wrcr.20503

simulators typically implement the single resistance, linear driving force model:

$$J = k_{la} \cdot a^n (C_s - C_w) \quad (1)$$

where J $[ML^{-3}T^{-1}]$ is the mass flux from the DNAPL to the water phase, k_{la} $[L/T]$ is the mass transfer coefficient, a^n $[1/L]$ is the effective normalized interfacial area between the DNAPL and the water phase, $C_s[M/L^3]$ is the effective solubility of the DNAPL, $C_w[M/L^3]$ is the bulk aqueous phase concentration, and $C_s - C_w$ is the difference in concentration between the DNAPL-water interface and the bulk aqueous phase.

[4] To predict the dissolution flux using equation (1), interfacial area estimates are needed. Such estimates are also needed to experimentally determine k_{la}. In the absence of ways to measure interfacial areas, the traditional approach has been to lump the mass transfer coefficient and the interfacial area into a single coefficient $K_L = k_{la} \cdot a^n [1/T]$, and then develop empirical correlations that relate system variables to the modified Sherwood number, $Sh' = K_L d_m^2 / D^*$, where d_m $[L]$ is the mean particle diameter and $D^*[L^2/T]$ is the molecular diffusion coefficient. Such correlations have been developed by many studies under a variety of experimental conditions [*Miller et al*., 1990; *Powers et al*., 1994b; *Imhoff et al*., 1994; *Saba and Illangasekare*, 2000; *Nambi and Powers*, 2003]. However, because these correlations are specific to the system they were developed in, they can be reliably extrapolated to different systems only when calibrated. Without proper calibration, extrapolation can lead to significant errors [*Powers et al*., 1992; *Nambi and Powers*, 2003]. This is rather restricting, since most correlations were developed in homogeneous systems of low dimensionality, for simple, emplaced source zones, while they are typically needed for heterogeneous systems of high dimensionality and DNAPL source zones of complex architecture.

[5] The above problems can be overcome by separately considering the mass transfer coefficient, k_{la}, and the interfacial area, a^n, when modeling dissolution. To predict k_{la}, *Pfannkuch* [1984] and *Powers et al*. [1994a] developed empirical models that relate the Sherwood number $(Sh = k_{la} d_m / D^*)$ to the aqueous phase velocity, v_x. However, the validity of these k_{la} models is uncertain, since they have not been sufficiently compared to experimental data, especially for complex DNAPL systems [*Powers et al*., 1994a; *Seagren et al*., 1999]. Validating k_{la} models is complicated, because it requires interfacial area estimates. Existing studies have used interfacial area estimates based on idealized geometries of DNAPL pools or ganglia [*Dekker and Abriola*, 2000; *Rathfelder et al*., 2001]. While it is likely that such idealizations do not reflect the complexity of real DNAPL source zones, the impact of this simplification on predicting dissolution rates has not been quantified thus far in the literature.

[6] Alternatively, interfacial areas can be modeled using the thermodynamic theory [*Morrow*, 1970]. The thermodynamic theory for interfacial areas is based on the principle that work done during DNAPL drainage and imbitition translates to the formation or destruction of DNAPL-water interfaces. This explicitly links interfacial areas to capillary pressure-saturation constitutive relationships, and renders the thermodynamic model suitable for REV-scale multiphase models, without requiring geometric assumptions or parameter calibration. The thermodynamic interfacial area model has shown potential to provide accurate estimates of interfacial areas [*Dobson et al*., 2006; *Porter et al*., 2010]. Recently, the approach was modified to incorporate saturation history [*Grant and Gerhard*, 2007a], and was utilized successfully to predict effluent concentrations from a two-dimensional DNAPL source zone [*Grant and Gerhard*, 2007b]. However, this study was performed at a low hydraulic gradient, so that changes in mass transfer rates were only caused by interfacial area variations, while the mass transfer coefficient was constant. At higher velocities, the mass transfer coefficient depends on water velocities and is affected by relative permeability and flow bypassing effects. These effects result in more complex mass transfer dynamics, and prevail in aquifers with high hydraulic gradients or significant flow focusing. The extent to which these effects impact depletion rates, and ultimately, the remediation potential of complex DNAPL source zones is not yet clearly understood.

[7] In this study, we present the first evaluation of the thermodynamically based dissolution model at high velocities, for complex DNAPL source zones, in three-dimensional heterogeneous systems. The model is tested using the experimental data set of *Zhang et al*. [2008], that includes high resolution, three-dimensional, local DNAPL saturations, as well as average and local effluent concentrations, obtained from experimental flow cells. To simulate dissolution, the thermodynamic model for interfacial areas is combined with the *Pfannkuch* [1984] k_{la} model. DNAPL infiltration is modeled using hysteretic DNAPL infiltration-redistribution constitutive relationships. The models are implemented within the multiphase numerical model COMPSIM [*Sleep and Sykes*, 1993], and simulations are performed without any parameter calibration, to evaluate the model's ability to predict dissolution based solely on soil properties and DNAPL release conditions, and for arbitrary source zone architectures. Upon validation of the model, the spatial and temporal variations of mass transfer rates are investigated and the controlling processes are identified. Finally, the results are compared to alternative models for both mass transfer coefficients and interfacial areas.

2. DNAPL Dissolution Experiments

[8] The bench-scale experiments presented by *Zhang et al*. [2008] were designed to evaluate the impact of soil heterogeneity and source zone architecture on DNAPL dissolution. The experiments were conducted in two three-dimensional flow cells, each packed with a different spatially correlated random permeability field. The two heterogeneous fields were generated so that they had the same transverse and vertical correlation lengths, but different longitudinal correlation lengths. In each of the two domains, 22.5 mL of DNAPL were allowed to infiltrate and equilibrate, and the DNAPL was then flushed with water under a constant head, until the DNAPL was completely dissolved. A unique attribute of the *Zhang et al*. [2008] experiments is the quantification of organic saturations in three dimensions during the course of dissolution, using ^{19}F

magnetic resonance imaging (MRI). Organic saturations at this level of detail have not been previously published and for the first time allow comparison with local saturations predicted by three-dimensional numerical modeling. In addition, aqueous concentrations were measured at nine separate outlets at the exit plane of the flow cells, enabling a comparison to both local and average dissolved concentrations.

[9] The *Zhang et al*. [2008] data set provides an excellent opportunity to validate the dissolution model for three main reasons. First, the experiments were conducted at a relatively high velocity ($\sim$1 m/d) and in three dimensions, conditions under which the model has not been previously evaluated, and that are highly relevant for field applications. Second, the DNAPL source zones were created so that they resemble a DNAPL release with complex architecture, unlike emplaced sources usually employed in DNAPL dissolution studies. Finally, the experiment was conducted in two different, well-characterized, heterogeneous domains. Evaluation of the dissolution model for both domains is used to test whether the model can predict dissolution from DNAPL source zones of arbitrary configuration and degree of heterogeneity.

[10] A brief description of the experimental methodology is presented in section 3.1. For further details on the experimental procedure, flowcell packing and imaging methods, the reader is referred to *Zhang et al*. [2007, 2008] and *Yoon et al*. [2008].

3. Numerical Simulations

3.1. Model Development and Boundary Conditions

[11] Multiphase flow and advective-dispersive transport was simulated using COMPSIM, a three-dimensional, multiphase, multicomponent, finite differences numerical model [*Sleep and Sykes*, 1993]. COMPSIM was designed, and has been extensively used, to simulate groundwater contamination and remediation of organic compounds [*McClure and Sleep*, 1996; *Sleep et al*., 2000; *O'Carroll and Sleep*, 2007, 2009]. The model solves the molar balance equation for each species and each phase. For multiphase flow, COMPSIM allows the use of infiltration models of varying complexity, from simple Brooks-Corey to the complex hysteretic constitutive relationships of *Gerhard and Kueper* [2003a, 2003b]. Mass transfer between phases is simulated using a source/sink term, which was modified for this work to incorporate a variety of rate-limited mass transfer formulations, including the *Pfannkuch* [1984] and *Powers et al*. [1994a] correlations and the interfacial area models evaluated.

[12] The simulated domain for each experiment included the entire 21 cm $\times$ 8.8 cm $\times$ 8.5 cm (length $\times$ width $\times$ height) flow cell, which was discretized in $62 \times 38 \times 33$ numerical blocks. The interior numerical grid was 0.25 cm $\times$ 0.25 cm horizontally, with vertical discretization varying between 0.21 and 0.31 cm, matching the resolution of the imaged organic saturations. The simulated permeability fields exactly matched the soil packing of the experimental flowcells, which consisted of $14 \times 8 \times 8$ physical 1 cm^3 cubes and corresponded to two different random permeability fields, the first having a correlation length of 2.1 cm (Experiment 1), and the second having a correlation length of 1.1 cm (Experiment 2) [*Zhang et al*., 2008]. Porosities and permeabilities of the five silica sands of the experiments were used as reported in *Zhang et al*. [2008], and mean particle diameters and capillary pressure-saturation parameters were obtained from *Scroth et al*. [1996]. Since the domain was well characterized, a low dispersivity of 0.01 cm for each direction was used. The properties of 1,3,5-trifluorobenzene (TFB), the DNAPL used in the experiments, were either computed or measured by *Zhang et al*. [2008] and were used in the simulations as reported therein.

[13] The simulation of DNAPL infiltration and dissolution was conducted in three phases, consistent with the experimental procedure. First, 22.5 mL of TFB were released into the initially fully water-saturated domain. A constant flux boundary condition at the point of release was employed to control the amount of TFB injected and the injection duration. After the injection was complete, TFB was allowed to equilibrate for 10 h, by setting all boundaries as no flow. Following the equilibration period, water flushing was simulated by a constant flux boundary condition through the entire inlet plane of the flowcell and a constant head through the exit plane of the flowcell. These boundary conditions resulted in the average Darcy velocity of 1 m/d (1.15×10^{-5} m/s) employed in the experiments.

3.2. Simulating DNAPL Infiltration

[14] The spatial distribution of DNAPL source zones has been shown to have a critical impact on dissolution rates and downstream mass fluxes [*Sale and McWhorter*, 2001; *Christ et al*., 2006; *Fure et al*., 2006; *Lemke and Abriola*, 2006; *Suchomel and Pennell*, 2006; *Zhang et al*., 2008]. As such, knowledge of the DNAPL source zone architecture is an implicit requirement for the successful simulation of DNAPL dissolution. For this reason, an intermediate, but equally important objective of this work is to accurately model the DNAPL spatial distribution of the *Zhang et al*. [2008] experiments. Although models for DNAPL infiltration are frequently used in the literature, a quantitative comparison between measured and predicted DNAPL saturations in three dimensions has not been presented before. Previous comparisons in two dimensions have been difficult, either because image analysis did not allow for quantification of saturations [*Grant et al*., 2007a] or because of discrepancies between the imaging resolution and the REV [*Suchomel and Pennell*, 2006; *Christ et al*., 2012]. The MRI-based quantification of DNAPL saturations in *Zhang et al*. [2008], at a resolution close to the REV scale, allows for a direct, quantitative comparison to organic saturations predicted at the numerical grid scale.

[15] To capture the hysteresis and residual entrapment observed in the *Zhang et al*. [2008] experiments, appropriate constitutive relationships are needed. Considering hysteresis determines the distribution of the DNAPL between residuals and pools, which has been shown to affect dissolution rates [*Christ et al*., 2010]. *Gerhard and Kueper* [2003a] recently modified the standard Brooks-Corey model to include hysteresis and the concept of terminal pressure, i.e., the capillary pressure during imbibition at which entrapment and residual formation begins. Furthermore, residual saturations were defined as a function of saturation history. Relative permeability relationships

consistent with these $P_c - S_w$ relationships were also developed by *Gerhard and Kueper* [2003b]. The combined $P_c - S_w - k_{rN}$ model (hereafter termed the GK model) has been validated in one and two dimensions, and has been shown to give better results than van Genuchten and Brooks-Corey models that do not incorporate the terminal pressure [*Gerhard and Kueper*, 2003a; *Grant et al*., 2007a]. For these reasons, COMPSIM was modified to calculate capillary pressures and relative permeabilities based on the GK model.

[16] The modifications introduced by the GK model require additional soil parameters, beyond those of the standard Brooks-Corey-Burdine model. The $P_c - S_w$ properties for the sands used in the *Zhang et al*. [2008] experiments were independently measured by *Scroth et al*. [1996] for a hysteretic van Genuchten model and a nonhysteretic Brooks-Corey model. *Dobson et al*. [2006] also measured residual water saturations for the same sands. All parameters reported in these two studies that are applicable to the GK model were used as reported therein. The only additional parameters required for the GK $P_c - S_w$ model are the terminal pressure, P_T, the imbibition pore size distribution index, λ_i, and the emergence saturation, S_w^M. The terminal pressure P_T is a measure of hysteresis, and is quantified as a fraction of the entry pressure P_D. Here the ratio of P_D to P_T was set equal to the inverse ratio of the van Genuchten α's for drainage and imbibition, as reported in *Scroth et al*. [1996] (i.e., $P_D/P_T = \alpha_i/\alpha_d$), and was within the range of ratios reported in *Grant et al*. [2007a]. λ_i was assumed to be equal to λ_d. Finally, the emergence saturation S_w^M was assumed to be equal to S_w^{X*}, i.e., the water saturation that corresponds to the maximum DNAPL residual.

[17] The rest of the parameters required by the GK model are all associated with the DNAPL relative permeability model. Although these parameters have been shown to be important for DNAPL flow [*Gerhard and Kueper*, 2003c; *Grant et al*., 2007a, 2007b], they are not crucial for the experiments modeled here, as DNAPL saturations are compared at hydrostatic equilibrium. For this reason, the $k_{rN} - S_w$ parameter values were assumed to correspond to the equivalent Brooks-Corey $k_{rN} - S_w$ relationships, with the exception of the maximum relative permeability, k_{rN}^{max}, that was calculated based on d_m [*Grant et al*., 2007a]. The water relative permeability is modeled by the *Brooks and Corey* [1964] function. Table 1 provides the values used for the GK model parameters, as well as calculation methods and assumptions, where applicable.

Table 1. P_c-S_w Soil Properties

Soil Type	12/20	20/30	30/40	40/50
P_D(cm)[a]	5.42	8.66	13.03	19.37
P_T(cm)[b]	3.77	5.52	8.19	10.63
$\lambda_{d,i}$[c]	3.94	5.57	6.91	6.17
S_r[d]	0.0345	0.046	0.052	0.0575
S_w^M[e]	0.848	0.842	0.808	0.79
$1 - S_w^{X*}$[d]	0.152	0.158	0.192	0.21
k_{rN}^{max}[f]	0.87	0.64	0.51	0.41
S_r^k[g]	0	0	0	0
$\tau_{d,i}$[g]	1	1	1	1
$\Delta S_w^{*d,*i}$[g]	0	0	0	0

[a] *Scroth et al*. [1996].
[b] Calculated as a fraction of P_T.
[c] Assumed $\lambda_d = \lambda_i$.
[d] *Dobson et al*. [2006].
[e] Assumed $S_w^M = S_w^{X*}$.
[f] Calculated by equation (1) in *Grant et al*. [2007b].
[g] Assumed.

3.3. Simulating DNAPL Dissolution

[18] According to equation (1), the total dissolution rate from the DNAPL to the water phase is proportional to the mass transfer coefficient, k_{la}, and the DNAPL-water interfacial area, a^n. While the overall mass transfer rate within a REV represents the combined effect of these two variables, each of them is a separate physical quantity and needs to be described by a separate model.

[19] The mass transfer coefficient represents the rate at which DNAPL mass transfer occurs at the local scale. Generally, this rate is determined by both diffusive and advective forces [*Miller et al*., 1990]. However, at low water velocities, mass transfer is mostly driven by diffusion, and k_{la} can be assumed to be constant [*Pfannkuch*, 1984; *Seagren et al*., 1999]. In contrast, at higher velocities, the mass transfer coefficient increases with velocity. Because of the complexity of porous media, the relationship between the mass transfer coefficient and velocity has been described using empirical studies. *Pfannkuch* [1984] was the first to develop an empirical correlation between the Sherwood number, and the Peclet number ($Pe = v_x d_m/D^*$) to describe the dissolution of an emplaced DNAPL pool (equation (2)):

$$Sh = 0.55 + 0.025 \cdot Pe^{1.5} \tag{2}$$

[20] *Powers et al*. [1994a] also developed an empirical correlation between the Sherwood number and the Reynolds number ($Re = \rho_w v_x d_m/\mu$) to describe the dissolution of entrapped solid naphthalene spheres (equation (3)):

$$Sh = 36.8 \cdot Re^{0.654} \tag{3}$$

[21] While a lot of research has been conducted for determining similar empirical correlations for the lumped mass transfer coefficient, K_L, the *Pfannkuch* [1984] and *Powers et al*. [1994a] correlations are the only correlations developed for k_{la} in porous media. More importantly, neither of the two correlations has undergone rigorous validation, especially in complex DNAPL systems. *Seagren et al*. [1999] compared the *Pfannkuch* [1984] correlation to the local equilibrium assumption and to a constant k_{la} using a 1-D analytical model and published dissolution column data. However, the simplified modeling approach, the small number of data points and the series of assumptions involved in determining input parameters introduced significant uncertainty in the results.

[22] For the purposes of the present study, the *Pfannkuch* [1984] correlation is considered more appropriate because of the predominance of DNAPL pools in the *Zhang et al*. [2008] experiments. However, given the limited validation that the correlation has undergone, the *Powers et al*. [1994a] correlation is also evaluated. It is noted that for the velocity ranges of the experiments ($0 < Pe < 280$), equations (2) and (3) result in drastically different Sherwood

numbers, and are, therefore, expected to result in significantly different dissolution rates.

[23] The second variable contributing to the overall mass transfer rate is the DNAPL-water interfacial area. In this work, interfacial areas are calculated using the thermodynamic model. Based on the thermodynamics of a closed two-phase system for a reversible displacement of fluids, the total external work applied is equal to the total change in surface free energy [*Morrow*, 1970; *Bradford and Leij*, 1997]. Translating this application of the first law of thermodynamics to REV scale variables in porous media gives the changes in total interfacial area as a function of the area under the capillary pressure-saturation curve (i.e., external work), interfacial tension between liquids (i.e., change in surface energy) and the porosity of the porous medium.

[24] Recently, *Dobson et al*. [2006] and *Grant and Gerhard* [2007a], in two independent studies, modified the original thermodynamic model to enforce continuity between the drainage and imbibition interfacial areas, and to consider saturation history. *Grant and Gerhard* [2007a] further extended the thermodynamic model to calculate the effective specific interfacial area, and to consider energy dissipation. In addition, *Grant and Gerhard* [2007a] adapted their interfacial area model to be consistent with the GK constitutive relationships (section 3.2), such that hysteresis is fully considered. A simplified version of the *Grant and Gerhard* [2007a] model is given by equation (4):

$$a^n(S_w) = \psi \cdot E_d \cdot n \cdot \frac{\int_1^{S_w} P_c^D dS_w - \int_{S_w}^{S'_w} P_c^I dS_w}{\sigma_{nw}} \qquad (4)$$

where S_w is the water saturation, ψ is the ratio between the effective and total interfacial area, E_d is an energy dissipation factor, n is the porosity, P_c is the capillary pressure, D is for drainage, I is for imbibition, and σ_{nw} is the DNAPL-water interfacial tension. The limits of integration in equation (4) correspond the end points of the $P_c - S_w$ drainage and imbibition curves. S'_w is the reversal saturation (i.e., the organic saturation at reversal from drainage to imbibition), and is spatially variable within the source zone. For this reason, the thermodynamic interfacial area model needs to be combined with a hysteretic infiltration model that keeps track of the reversal saturations, such as the GK model utilized here.

[25] The thermodynamic interfacial area model has been shown to provide good estimates of measured effective interfacial areas [*Grant and Gerhard*, 2007a; *Dobson et al*., 2006; *Porter et al*., 2010], and has been validated for a complex DNAPL source zone in a 2-D heterogeneous domain, with low water velocities [*Grant and Gerhard*, 2007b]. However, the model has never been tested in systems with higher velocities. In such cases, the dynamics of mass transfer are more complex, and the relative role of interfacial areas and mass transfer coefficients is not clear. Furthermore, the thermodynamic model has not been previously compared with geometric interfacial area models [e.g., *Powers et al*., 1991]. These relationships are investigated here with reference to the *Zhang et al*. [2008] experiments. The values of the soil properties used in equation (4) are reported in Table 1. The interfacial tension σ_{nw} for TFB is 32.86 dynes/cm [*Zhang et al*., 2008], and following *Grant and Gerhard* [2007a], $E_d = 0.21$ was assumed, and ψ was calculated as a polynomial function of water saturation. The combination of the thermodynamic interfacial area model of *Grant and Gerhard* [2007a] and the *Pfannkuch* [1984] correlation for k_{la} will be referred to as the base case.

3.4. Mass Transfer Limiting Processes

[26] Mass transfer limitations are often held responsible for the persistence of DNAPLs in the subsurface. However, the specific processes and conditions that result in deviations from equilibrium dissolution are not clear. Such deviations and their causes are likely to vary in space, especially in DNAPL source zones with complex architectures. The spatial detail provided by the multiphase numerical model employed herein is used to answer these questions. Mass transfer limitations are quantified by comparison to simulations assuming local equilibrium between the DNAPL and the aqueous phase. Such comparisons have been performed in previous studies, and while in some cases, equilibrium greatly overestimated dissolved concentrations [*Unger et al*., 1998], in other cases, it provided good agreement to experimental data [*Nambi and Powers*, 2003] or numerical simulations [*Dekker and Abriola*, 2000]. The underlying causes for this behavior are investigated here by identifying the processes responsible for mass transfer limitations in the *Zhang et al*. [2008] experiments. The respective effects of mass transfer coefficients and interfacial areas on the spatially variable mass transfer rates are evaluated for the base case. Then, alternative models for both parameters are compared and the implications of the model choice are shown in each case.

4. Results

4.1. Source Zone Architecture

[27] The model's ability to predict the source zone architecture at equilibrium and during dissolution is evaluated for the long correlation length flowcell of *Zhang et al*. [2008] (Experiment 1). This analysis is conducted (a) to evaluate the ability of the GK infiltration model to quantify organic saturations and (b) to investigate features of the predicted source zone architecture that might influence dissolution kinetics. The comparison is performed against the experimentally measured organic saturations at select times using five metrics: (a) local grid-scale saturations, (b) DNAPL volume in each horizontal layer, (c) DNAPL saturations summed over the y direction, (d) maximum length of the source zone in the each direction, and (e) the ganglia fraction.

[28] The measured and predicted organic saturations at $t = 0$ are shown in Figures 1a and 1b, for three cross sections of the flowcell. At this time, before flushing has started, the predicted saturations are determined by the GK constitutive relationships and are not affected by the dissolution model. The results indicate that the model effectively captured the main features of the source zone. However, the model predicted a more uniform distribution of the DNAPL, which spread through the full extent of the most permeable sand. In contrast, the experimental saturations did not spread as much, as higher organic saturations were

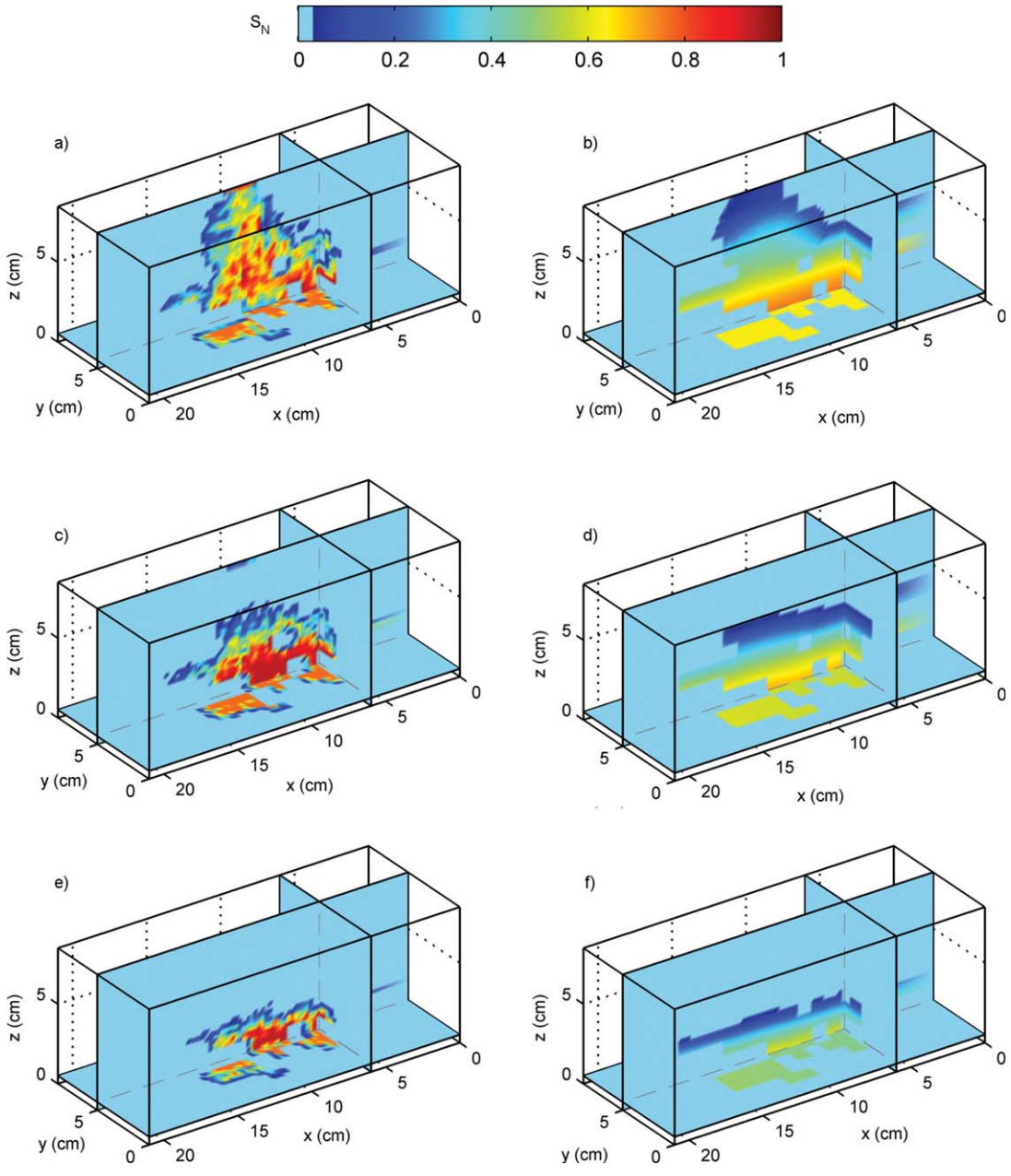

Figure 1. DNAPL saturations (a) measured at $PV = 0$, (b) predicted at $PV = 0$, (c) measured at $PV = 70$, (d) predicted at $PV = 70$, (e) measured at $PV = 170$, and (f) predicted at $PV = 170$. Flow is from right to left.

trapped along the infiltration path. The overprediction of the source horizontal extent by the model inevitably resulted in DNAPL pools with lower organic saturations than those observed. The excessive trapping and heterogeneities in the observed organic saturations likely reflect small scale heterogeneities within the same soil type. Since the model did not account for such heterogeneities, the observed discrepancies are reasonable. It is also possible that during the packing of the flowcell, mixing occurred at the interfaces between fine and coarse sands, as also suggested by *Yoon et al*. [2008]. Such mixing is also not accounted for by the model, and may contribute to the observed discrepancies between the experimental and predicted organic saturations.

[29] Discrepancies at the end of the infiltration period are also propagated to later times during dissolution (Figures 1c–1f). Despite this, the experiment and the model show a remarkably similar decline in the vertical extent of the source zone, and slower changes in its horizontal extent as the DNAPL dissolves. This behavior reflects the higher rates of dissolution at the top boundary of the source zone, where the flow is not impeded by the presence of DNAPL. The close reproduction of the evolution of the source zone in time indicates that the model was able to predict the spatial variability of dissolution rates.

[30] In terms of the vertical DNAPL mass distribution, the model was within 0.5 mL of the observed total DNAPL volume in each horizontal layer (2.2% of total DNAPL), at

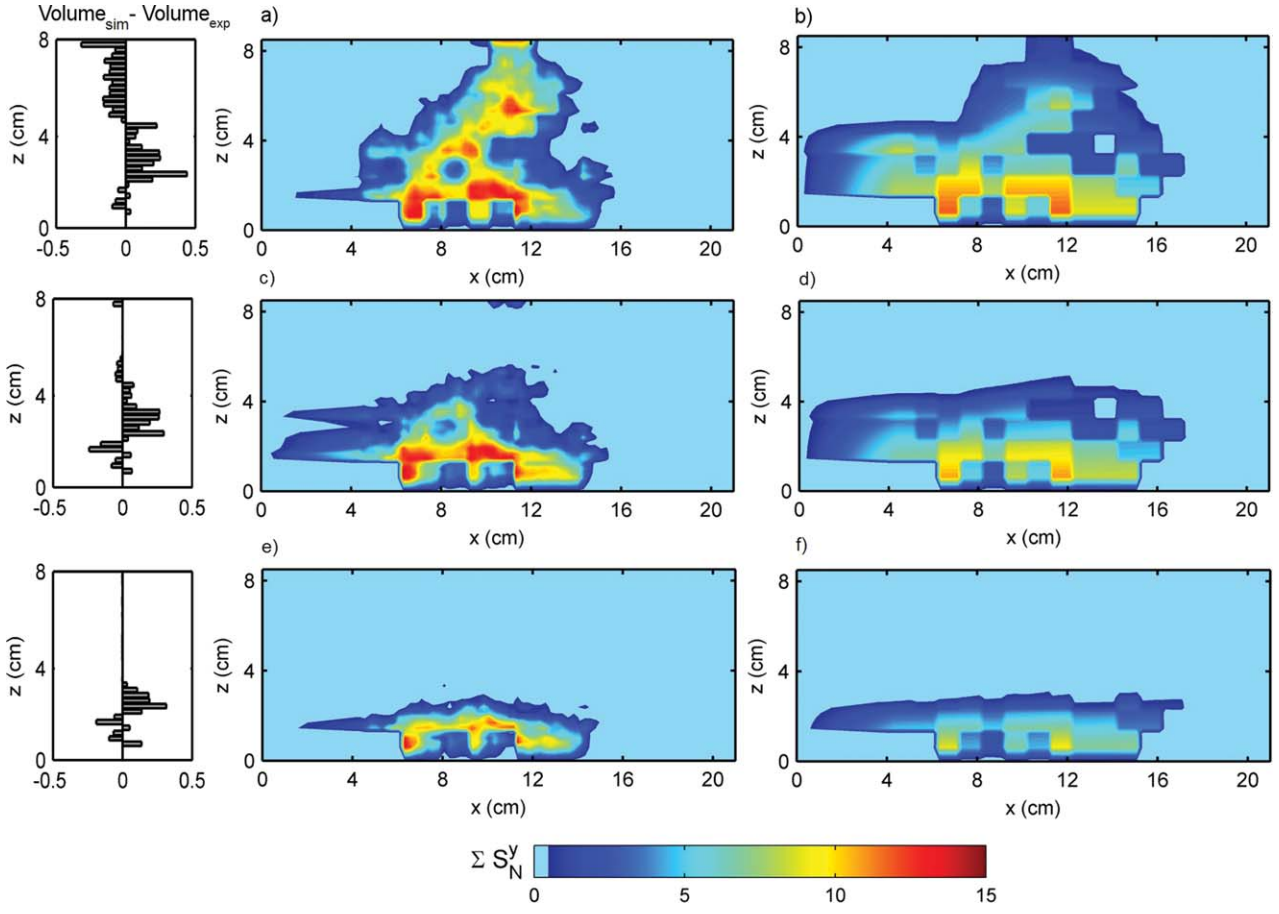

Figure 2. DNAPL saturations summed over the y direction (flow from left to right) (a) measured at $PV = 0$, (b) predicted at $PV = 0$, (c) measured at $PV = 70$, (d) predicted at $PV = 70$, (e) measured at $PV = 170$, and (f) predicted at $PV = 170$. Bar graphs on the left indicate the difference between predicted and measured DNAPL volume (mL) for each horizontal layer simulated.

all times. This can be seen in the bar graphs of Figure 2, which show the absolute difference (in mL) between the DNAPL volume simulated and the DNAPL volume observed in each horizontal layer of the flowcell. The contour plots in Figure 2 illustrate measured and predicted DNAPL saturations, summed over the y direction at three different times. Here the overprediction of the DNAPL spread in the flow direction is more clear. However, it can also be seen that the model correctly predicted the features of the source zone that potentially resulted in significant flow bypassing, both earlier and later in time.

[31] The measured and predicted source zone extent during dissolution is also compared in Figure 3, where the maximum length of the source zone in each of the x, y, and z directions is plotted with time. The maximum length is defined as the maximum distance over which blocks with $S_N > 0.15$ are connected. This figure shows that the model closely matched the maximum vertical depth of the source zone at all times. In the y direction, the model slightly overestimated the maximum extent by about 1 cm for the first 100 pore volumes. The largest discrepancy is in the direction of the flow (x direction), and reflects the overestimation of the DNAPL spread described earlier.

[32] Finally, Figure 4 shows the ganglia fraction (GF) for measured and modeled DNAPL saturations. The ganglia fraction is the commonly used ganglia-to-pool ratio (GTP) re-expressed as a percentage, such that $GF = GTP/(1 + GTP)$. The GTP is calculated on a mass basis, i.e., the total DNAPL mass in blocks with $S_N < S_{N,threshold}$, divided by the total DNAPL mass in blocks with $S_N > S_{N,threshold}$. The value for $S_{N,threshold}$ was chosen to be equal to the maximum residual DNAPL saturation, calculated as $1 - S_w^{X*}$, which is equal to 0.152 for Accusand 12/20 (Table 1). As Figure 4 shows the proportion of low to high saturations is closely reproduced by the model for the whole duration of the experiment.

[33] The above comparisons indicate that the model predicted the source zone architecture reasonably well, except in the magnitude of DNAPL pool saturations and the spread of the source zone in the flow direction. These mismatches are expected to have a limited impact on the effluent concentrations predictions, because (a) the DNAPL pool saturations have a small impact on effluent concentrations due to relative permeability effects and (b) the larger extent of the source zone in the flow direction does not increase flow bypassing due to the low predicted saturations at the extremities of the source zone. On the contrary, effluent concentrations are expected to be more sensitive to the DNAPL extent in the directions perpendicular to the flow, and the saturations at the top boundary of the source

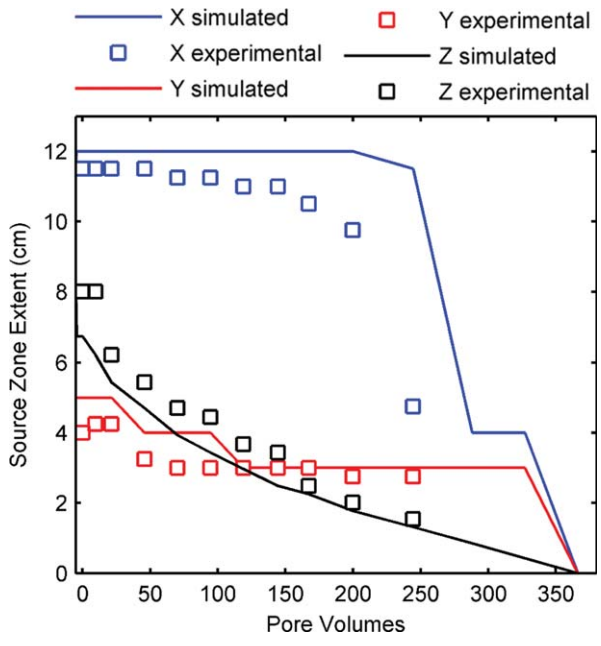

Figure 3. Measured (squares) and predicted (solid lines) maximum source zone extent in the x, y, and z directions during dissolution in Experiment 1.

zone, both of which were closely reproduced by the model. These hypotheses will be evaluated in the following sections.

4.2. Effluent Concentrations

[34] Effluent concentrations observed downgradient from a DNAPL source zone reflect the aggregate effect of local dissolution rates at DNAPL-water interfaces. In this section, the dissolution model is evaluated by comparing measured and predicted effluent concentrations at the downgradient end of the *Zhang et al*. [2008] flowcells, during the course of dissolution. The modeled effluent concentrations are based on the distribution of the DNAPL predicted by the GK infiltration model, and therefore, the evaluation of the dissolution model is performed given the discrepancies in DNAPL distribution described in section 4.1. Although these discrepancies will affect the predictions of the dissolution model, evaluating the combined infiltration-dissolution model without using information on the measured DNAPL saturations is intended to show the purely predictive ability of the model, relying solely on knowledge of soil properties and DNAPL release conditions.

[35] Initially, effluent concentrations averaged over the whole exit plane of the flowcells are compared. Experimentally, these concentrations were measured by collective sampling from nine separate ports, corresponding to nine outlet chambers of equal area located at the exit plane of the flowcell. Numerically, this corresponds to flux-averaging local concentrations for each one-ninth of the exit plane and arithmetically averaging the nine flux averages. Figure 5 shows measured average concentrations, together with concentrations predicted by the base case dissolution model (*Pfannkuch* [1984] correlation and thermodynamic interfacial area model). The predicted concentrations closely follow both the magnitude and the temporal changes of the measured concentrations, such as the increase during the early stage of the Experiment 2 and the decreases in concentration reductions at later stages of both experiments.

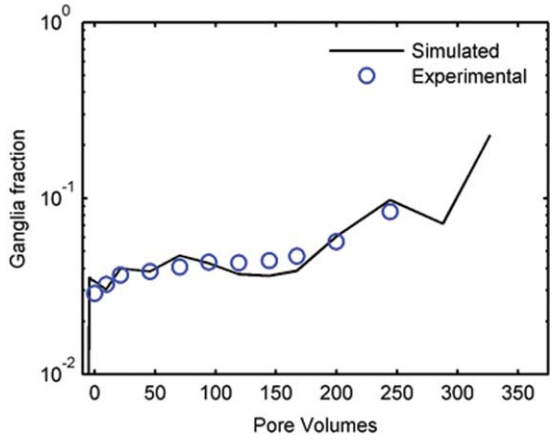

Figure 4. Measured (circles) and predicted (solid line) ganglia to pool mass fraction during dissolution in Experiment 1.

[36] The initial increase in concentrations, which was more pronounced in Experiment 2, has been previously attributed to decreasing DNAPL saturations and increasing contact between DNAPL and water [*Zhang et al*., 2007]. However, the thermodynamic interfacial area model employed here did not predict an increase in interfacial areas; it rather showed a monotonic decrease in total effective interfacial areas for the whole duration of both experiments (Figure 6). The initial increase in concentrations was rather a result of the flow dynamics in the flowcell and the impact on mass transfer coefficients: the equilibrated DNAPL, being at its maximum spread at $t = 0$, caused the maximum flow bypassing. Flow bypassing resulted in low initial concentrations downstream. As the flowcell was being flushed, preferential flow occurred through the low-saturation top of the source zone (Figure 1). The decreasing DNAPL saturations in this area resulted in increasing relative permeabilities and aqueous velocities and finally in higher mass transfer coefficients k_{la} (equation (2)) and dissolved concentrations. This behavior is consistent with previous observations by *Powers et al*. [1998] and *Nambi and Powers* [2000].

[37] The increase in initial concentrations ceases when the vertical extent of the source zone starts decreasing due to dissolution. At that point, even though increases in mass transfer and concentrations still occur in regions of low saturations, they are counteracted by the increasing dilution of the average effluent concentration with time. Depending on which of the two processes dominates, the effluent concentrations go through fast or slow reductions. This also explains the contrasting behavior of initial concentrations between Experiments 1 and 2. In Experiment 1, the low saturations at the upper part of the flowcell dissolved fast, and the vertical extent of the source started decreasing within the first few pore volumes. In contrast, the DNAPL in Experiment 2 was trapped at higher saturations in the upper part of the flowcell, such that the source zone size only

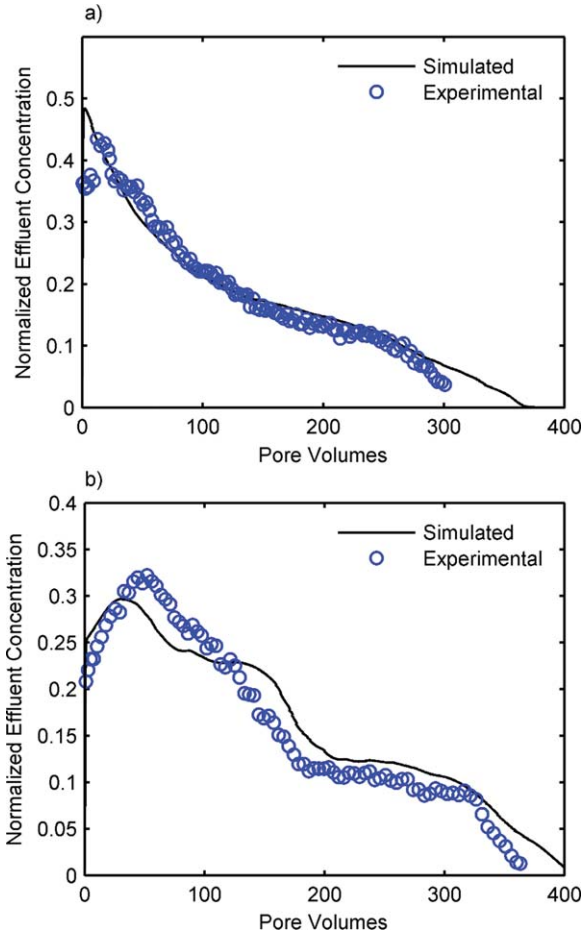

Figure 5. Measured (circles) and predicted (solid lines) average effluent concentrations, for (a) Experiment 1 (long correlation length) and (b) Experiment 2 (short correlation length).

started reducing after 25 PV, leading to the decrease in effluent concentrations.

[38] These temporal changes in concentrations are further depicted in Figure 7, which show the measured and predicted concentrations at three outlet ports, corresponding to the top, middle, and bottom center of the flowcell. The center ports accounted for most of the flow, and therefore, had the biggest impact on the overall average concentrations. Although the model did not exactly match the magnitude of local concentrations, it closely predicted the temporal changes, such as the pattern of initially increasing concentrations followed by decreasing concentrations. It also matched the relatively lower concentrations at the bottom port, which was due to increased flow bypassing at the bottom third of the flowcell where DNAPL pooled. The local concentrations further illustrate the processes that determined the average concentrations. For example, in Experiment 1, the concentrations in the upper parts of the flowcell rapidly decreased because the source zone in this region was depleted within the first few pore volumes. This rapid decrease could not be compensated by the slower increase at the bottom port. In contrast, in Experiment 2, between 200 and 300 PVs, the increasing mass transfer in the bottom third of the domain counteracted the decrease in

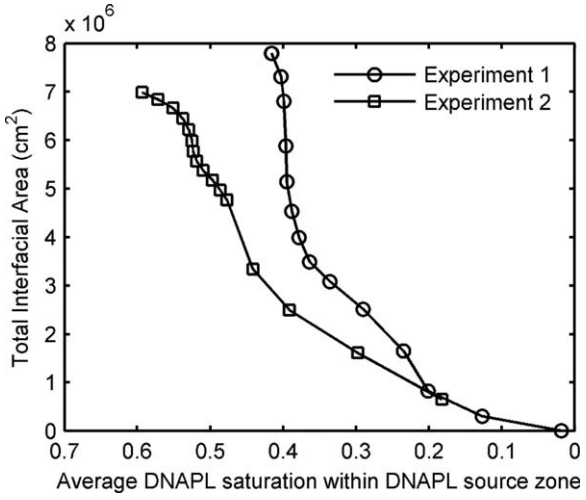

Figure 6. Predicted total interfacial areas versus average DNAPL saturation within the source zone for Experiments 1 and 2.

concentrations from the middle third of the domain and resulted in a relatively constant average concentration.

[39] The successful prediction of the temporal changes in concentrations is a result of capturing the main features of the source zone architecture. On the other hand, the features of the source zone that were not predicted correctly by the model can explain the discrepancies in the magnitude of concentrations. The overprediction of top and middle port concentrations is the result of the model underpredicting the saturations, and thus overpredicting the velocity and mass transfer rates in the top and middle third of the cell. In contrast, the underprediction of saturations at the lower third of the domain did not impact mass transfer rates, as the predicted saturations were high enough to cause almost complete flow bypassing. However, the overprediction of the DNAPL longitudinal spread in this lower area still resulted in the underprediction of the bottom port concentrations. In the simulation, the DNAPL completely filled the most permeable soil type in the bottom third of the cell, such that locations adjacent to the DNAPL had lower intrinsic soil permeability and, therefore, lower velocities, which resulted in low concentration gradients and low mass transfer rates. In the experiment, the lesser DNAPL spread allowed the development of high velocities within the DNAPL-free highly permeable soil type, which considerably increased the concentration gradients at the DNAPL-water interface and led to faster mass transfer and higher concentrations than those predicted by the model.

[40] The above reflect the effluent concentrations sensitivity to velocity, preferential flow, and source zone architecture. It should also be noted that the discrepancies between the model and the experiment cumulatively increase with time and distance travelled, reaching a maximum at the exit of the flowcell, where concentrations were measured. Given the complexity of the flowpaths in the *Zhang et al*. [2008] experiments, the agreement between measured and predicted port concentrations shown in Figure 7 is satisfactory, as the main features of the breakthrough curves (e.g., peak arrival times, nonmonotonic behavior) are captured and the average behavior is closely

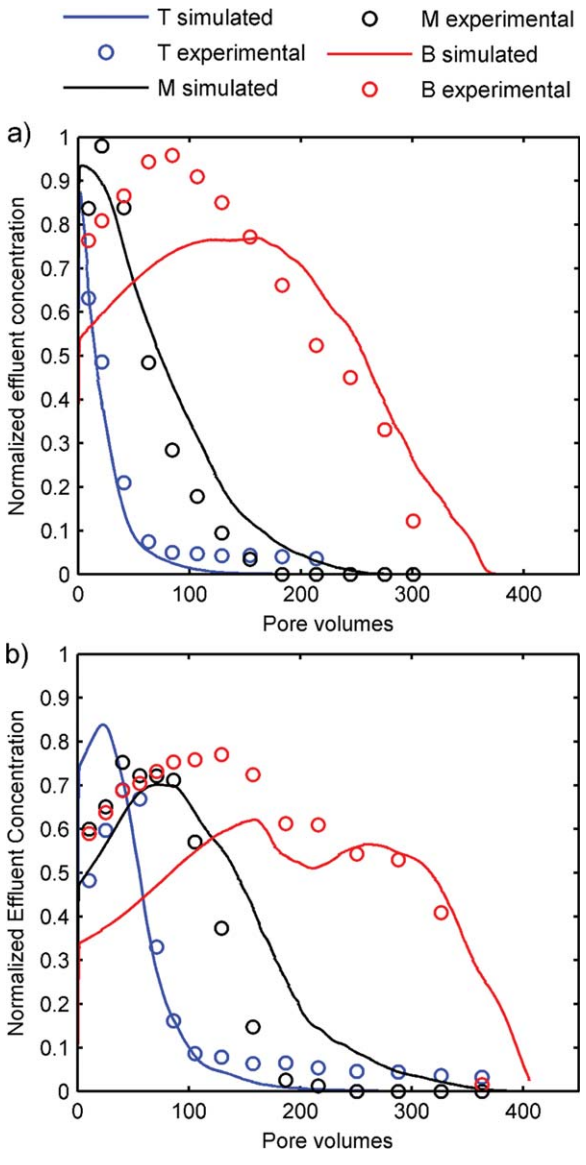

Figure 7. Measured (circles) and predicted (solid lines) effluent concentrations for center ports of the flow cell (T: Top, M: Middle, and B: Bottom), for (a) Experiment 1 and (b) Experiment 2.

reproduced. Most importantly, the effluent concentrations were predicted by the model without requiring any calibration, signifying the model's ability to capture the important physical processes, for arbitrary source zone architectures.

4.3. Mass Transfer Limiting Processes

[41] Having established that the simulations are representative of the mass transfer process in the *Zhang et al*. [2008] experiments, the impact of DNAPL saturations on local mass transfer rates, and on the overall depletion of the source zone is investigated. The contribution of each parameter of equation (1) to the overall dissolution is evaluated, by separately analyzing the spatial distributions of interfacial areas and mass transfer coefficients.

[42] Figure 8 illustrates these distributions for the same *x*-*z* plane shown in Figure 1 ($y = 5$ cm, note different orientation of the x axis). DNAPL-water interfacial areas (Figure 8, a^n, first column) show a correspondence with DNAPL saturations at all times during dissolution (Figure 1, second column), with interfacial areas being the highest at the bottom of the domain, and the lowest at the top boundary of the DNAPL. In contrast, aqueous velocities show the opposite trend: at low DNAPL saturations, relative permeabilities and velocities are high, while they considerably decrease at DNAPL pools. Since the mass transfer coefficient, k_{la}, is a strong function of velocity (equation (2)), the product $a^n \cdot k_{la}$ (Figure 8, second column) is low for DNAPL pools at the bottom of the system, higher at the top of the source zone, and near zero at the top extremities of the source zone. As such, the spatial distribution of the overall mass transfer rate is affected by the distribution of both mass transfer coefficients and interfacial areas. Regions with organic saturations between 5 and 30% show the highest mass transfer rates, while higher saturations are associated with as much as an order of magnitude decrease in mass transfer rates, due to reductions in relative permeability. At high saturations, concentration gradients are also near zero due to low velocities and prolonged contact with DNAPL (Figure 8, third column). This further reduces the active mass transfer from high saturation regions, and illustrates the important role of low to medium saturations. It also demonstrates that the dissolution rates and overall mass discharge are sensitive to the aqueous flow field, as affected by the presence of the DNAPL phase and the resulting reductions in relative permeabilities, and corroborates previous findings by *Zhang et al*. [2008], where simplified models not accounting for such reductions did not reproduce effluent concentrations adequately.

[43] Based on the above, the mass transfer coefficient, k_{la}, and its dependency on velocity play a crucial role on the magnitude and spatial distribution of dissolution rates. This conclusion was reached for the base case simulation, which utilized the *Pfannkuch* [1984] correlation (equation (2)). Because of the limited testing that this correlation has undergone in complex DNAPL systems, and to evaluate the impact of the k_{la} model on dissolution and effluent concentrations, three additional models were tested: (a) the local equilibrium model, which implies an infinite k_{la}, (b) a constant k_{la} model calculated for the average velocity with the *Pfannkuch* [1984] correlation, and (c) the *Powers et al*. [1994a] correlation (equation (3)).

[44] The results for the different k_{la} models are shown in Figure 9. Both the *Powers et al*. [1994a] and the constant k_{la} models underpredicted the concentrations for both experiments and did not capture either the concentration changes, or the DNAPL extinction time. This is because the *Powers et al*. [1994a] correlation has a weak dependence on velocity, producing lower and more uniform mass transfer rates than the *Pfannkuch* [1984] correlation. The difference between the two correlations increases with higher velocities and lower organic saturations. Similarly, the constant k_{la} model underpredicted the local mass transfer rates in the critical high-velocity region, due to its insensitivity to flow focusing and changes in local velocities. The consequences of underpredicting mass transfer are better illustrated in terms of the time to complete DNAPL removal; the *Powers et al*. [1994a] correlation overpredicted the time to complete removal by about 100

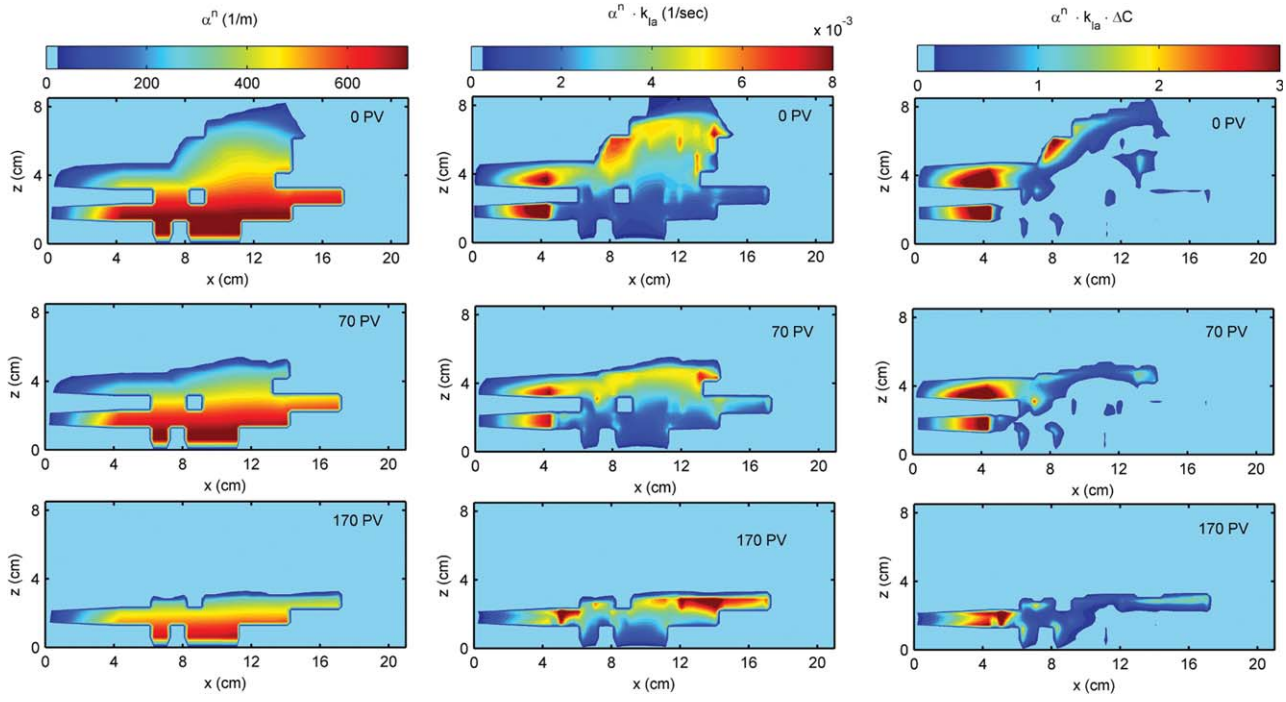

Figure 8. Simulated interfacial areas, mass transfer rates and solute mass fluxes from the DNAPL source zone (base case simulation). Results are shown at $y = 5$ cm, at 0, 70, and 170 PV. Flow is from left to right.

PV compared to the base case simulation for Experiment 1, even though the initial concentration difference was less than 10% of the saturation limit. Comparing the two experiments, Experiment 2 was more sensitive to the k_{la} model, because of its more complex DNAPL architecture and hydrodynamics, which resulted in more flow bypassing, and more variable local velocities. Finally, the simulation that assumed local equilibrium predicted concentration profiles relatively close to the base case kinetic model, indicating that near-equilibrium conditions were reached in the two experiments. However, since the local equilibrium model assumes maximum mass transfer everywhere in the source zone, neglecting the impact of low interfacial areas and low relative permeabilities on mass transfer rates, it overestimated experimental concentrations and underpredicted DNAPL extinction times. Overall, among the k_{la} models evaluated, the base case simulation implementing the *Pfannkuch* [1984] correlation resulted in the best fit for concentrations and the lowest root mean square error (RMSE) for both experiments.

[45] To investigate the impact of the interfacial area model on the results, the thermodynamic interfacial area model was compared to the sphere model of *Powers et al*. [1991]. The sphere model calculates specific interfacial areas assuming that the DNAPL in each numerical block is present as one or more spheres, with a radius that is a function of DNAPL saturation. A constant factor is used to correct the area for DNAPL-soil interfaces. *Dekker and Abriola* [2000] employed this method and calculated the number of spherical blobs based on the initial saturation and the soil mean particle diameter, keeping it constant during dissolution. In the present work, the same constant number of blobs is assumed for every numerical block, and the impact of this assumption is tested.

[46] Simulations were conducted using a single, two, and three-sphere model for interfacial areas, combined with the *Pfannkuch* [1984] correlation. The areas predicted by all sphere models were higher than those predicted by the thermodynamic model, with the difference increasing with organic saturation and number of blobs. As a result, the predicted mass transfer rates were higher, with the effluent concentrations progressively reaching equilibrium levels as the number of blobs was increased (Figure 10). Among the sphere models evaluated, the single-sphere model predicted concentrations that are closer to the base case simulation and the experiment. However, the assumption of a single DNAPL blob for every numerical block may be unrealistic. On the other hand, increasing the number of blobs to three or more would result in equilibrium dissolution. These observations are based on the assumption that the number of blobs is spatially and temporally constant. If the number of blobs per block was to be spatially varied with the DNAPL saturation according to the method of *Dekker and Abriola* [2000], any block with organic saturation greater than 10% would have had more than three blobs, and the model would have resulted in equilibrium dissolution.

[47] The above results illustrate that the number of DNAPL blobs in each numerical block is an important parameter for the sphere model. According to *Dekker and Abriola* [2000], the number of blobs, and therefore, the interfacial areas, increase fast with decreasing mean particle diameter $\left(\propto 1/d_m^3\right)$ [*Dekker and Abriola*, 2000]. On the contrary, the thermodynamic model calculates interfacial areas based on the capillary pressure, which varies less

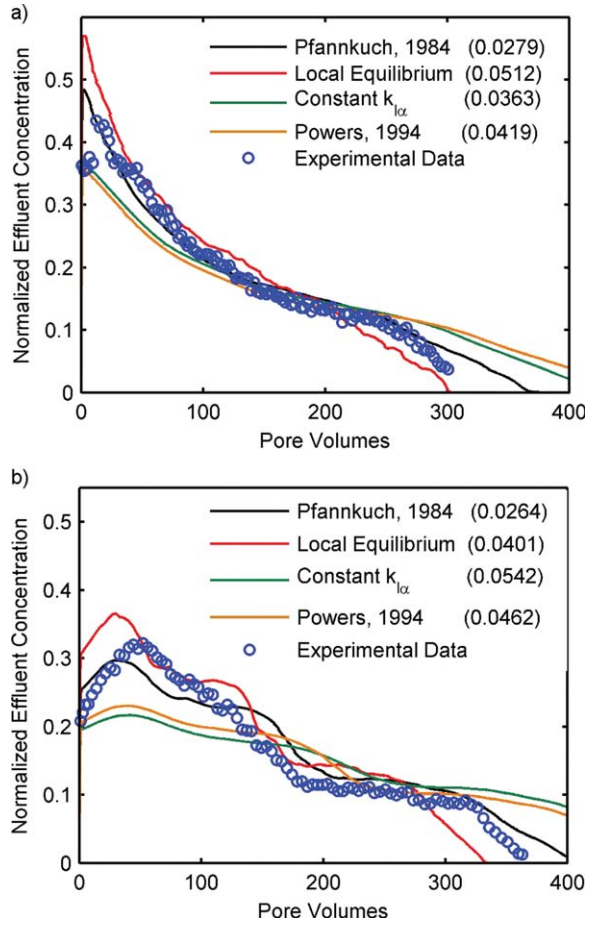

Figure 9. Measured (circles) and predicted (solid lines) average effluent concentrations for the four different k_{la} models, for (a) Experiment 1 and (b) Experiment 2. Numbers in parentheses indicate RMSEs.

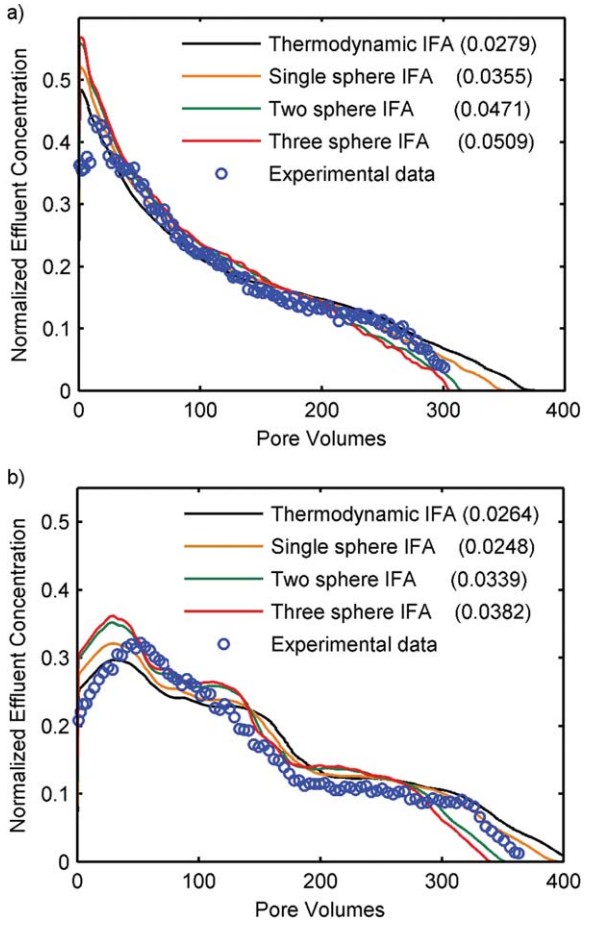

Figure 10. Measured (circles) and predicted (solid lines) average effluent concentrations for the thermodynamic interfacial area (IFA) model and geometric sphere models, for (a) Experiment 1 and (b) Experiment 2. Numbers in parentheses indicate RMSEs.

dramatically with the mean particle diameter ($\propto 1/d_m$). As a result, the discrepancies between the sphere model and the thermodynamic model will increase for less permeable soils, with the sphere model being more likely to result to equilibrium dissolution. Based on the above, it is concluded that the thermodynamic model is more suitable to capture the magnitude of the interfacial areas and associated mass transfer limitations, although further research is needed to confirm this.

5. Summary and Conclusions

[48] A three-dimensional multiphase numerical model was used to simulate the infiltration and dissolution of a complex DNAPL source zone in two heterogeneous, well-characterized experimental flow cells. The model employed hysteretic Brooks-Corey-Burdine capillary pressure-saturation-relative permeability relationships to simulate DNAPL infiltration. Dissolution was modeled considering velocity-dependent mass transfer coefficients based on the *Pfannkuch* [1984] correlation, and interfacial areas calculated according to thermodynamic theory. The most important attribute of the model is that it is purely predictive, as it does not require calibration of any parameters, and only requires information on soil properties and DNAPL release conditions.

[49] The model closely predicted average effluent concentrations for the two dissolution experiments. This was a result of the model's ability to reproduce both the main features of the DNAPL spatial distribution and the local dissolution rates. This coupled modeling methodology allowed for a detailed evaluation of the interdependence between the source zone architecture and the effluent concentrations. The source zone architecture was found to have a pronounced influence on mass transfer rates through its effect on aqueous relative permeabilities. It was shown that dissolution from low to medium organic saturations contributed the most to DNAPL depletion, while saturations higher than 30% were related to lower mass transfer rates and slower DNAPL depletion.

[50] The importance of the mass transfer dependence on velocity was demonstrated by evaluating three models, in addition to the *Pfannkuch* [1984] model. The spatial variability of mass transfer rates drastically affected the overall dissolution in high velocity conditions, and simplifying assumptions (e.g., equilibrium, constant mass transfer rate)

resulted in under or overpredicting DNAPL extinction times and mass discharge. For the experiments modeled in this work, the *Pfannkuch* [1984] k_{la} model predicted the experimental data better than the *Powers et al*. [1994a] model. Finally, the thermodynamic interfacial area model was compared to three diminishing sphere models and it was found that the latter predicted significantly higher interfacial areas, thus not capturing mass transfer limitations.

[51] This study represents the first validation of the thermodynamic interfacial area model combined with the *Pfannkuch* [1984] correlation for the simulation of DNAPL dissolution in three dimensions and for high aqueous phase velocities. The model closely predicted the mass discharge from two different complex DNAPL source zones, without relying on measured transient local DNAPL saturations that would typically be difficult to obtain, but relying solely on soil properties and DNAPL release conditions. The model's ability to predict dissolution without calibration indicates its applicability for arbitrarily complex systems and for conditions where high velocities may develop, such as in aggressive remediation operations, or highly heterogeneous aquifers. The model presents a unique opportunity to better understand the links between source zone architecture and DNAPL dissolution, while it also signifies the importance of accurate soil and source zone characterization. Further evaluation of the model in different systems will help solidify its validity, so that it can be utilized toward more reliable predictions of the remediation potential of DNAPL source zones.

[52] **Acknowledgments.** The assistance of Changyong Zhang and Hongkyu Yoon with the processing and analysis of experimental data is gratefully acknowledged. This research was financially supported by the Natural Sciences and Engineering Research Council (NSERC) of Canada, as well as an Ontario Graduate Scholarship (OGS) for the first author. Funding was also provided by DuPont. We would also like to thank the editor, associate editor, and the three anonymous reviewers for their helpful suggestions on improving our manuscript.

References

Bradford, S., and F. Leij (1997), Estimating interfacial areas for multi-fluid soil systems, *J. Contam. Hydrol.*, *27*(1–2), 83–105.

Brooks, R. H., and A. T. Corey (1964), Hydraulic properties of porous media, *Hydrol. Pap. 3*, Civ. Eng. Dep., Colo. State Univ., Fort Collins.

Christ, J. A., C. A. Ramsburg, K. D. Pennell, and L. M. Abriola (2006), Estimating mass discharge from dense nonaqueous phase liquid source zones using upscaled mass transfer coefficients: An evaluation using multiphase numerical simulations, *Water Resour. Res.*, *42*, W11420, doi:10.1029/2006WR004886.

Christ, J. A., C. A. Ramsburg, K. D. Pennell, and L. M. Abriola (2010), Predicting DNAPL mass discharge from pool-dominated source zones, *J. Contam. Hydrol.*, *114*, 18–34.

Christ, J. A., K. D. Pennell, and L. Abriola (2012), Quantification of experimental subsurface fluid saturations from high-resolution source zone images, *Water Resour. Res.*, *48*, W01517, doi:10.1029/2011WR010400.

Dekker, T. J., and L. M. Abriola (2000), The influence of field-scale heterogeneity on the surfactant enhanced remediation of entrapped nonaqueous phase liquids, *J. Contam. Hydrol.*, *42*, 219–251.

DiFilippo, E. L., K. C. Carroll, and M. Brusseau (2010), Impact of organic-liquid distribution and flow field heterogeneity on reductions in mass flux, *J. Contam. Hydrol.*, *115*, 14–25.

Dobson, R., M. H. Schroth, M. Oostrom, and J. Zeyer (2006), Determination of NAPL-water interfacial areas in well-characterized porous media, *Environ. Sci. Technol.*, *40*, 815–822.

Fure, A. D., J. W. Jawitz, and M. D. Annable (2006), DNAPL source depletion: Linking architecture and flux response, *J. Contam. Hydrol.*, *85*, 118–140.

Gerhard, J. I., and B. Kueper (2003a), Capillary pressure characteristics necessary for simulating DNAPL infiltration, redistribution and immobilization in saturated porous media, *Water Resour. Res.*, *39*(8), 1212, doi:10.1029/2002WR001270.

Gerhard, J. I., and B. Kueper (2003b), Relative permeability characteristics necessary for simulating DNAPL infiltration, redistribution and immobilization in saturated porous media, *Water Resour. Res.*, *39*(8), 1212, doi:10.1029/2002WR001270.

Gerhard, J. I., and B. Kueper (2003c), Influence of constitutive model parameters on the predicted migration of DNAPL in heterogeneous porous media, *Water Resour. Res.*, *39*(10), 1279, doi:10.1029/2002WR001570.

Grant, G. P., and J. I. Gerhard (2007a), Simulating the dissolution of a complex DNAPL source zone: 1. Model to predict interfacial area, *Water Resour. Res.*, *43*, W12410, doi:10.1029/2007WR006038.

Grant, G. P., and J. I. Gerhard (2007b), Simulating the dissolution of a complex DNAPL source zone: 2. Experimental validation of an interfacial area-based mass transfer model, *Water Resour. Res.*, *43*, W12409, doi:10.1029/2007WR006039.

Grant, G. P., J. I. Gerhard, and B. Kueper (2007a), Multidimensional validation of a numerical model for simulating a DNAPL release in heterogeneous porous media, *J. Contam. Hydrol.*, *92*, 109–128.

Grant, G. P., J. I. Gerhard, and B. Kueper (2007b), Field scale impacts of spatially correlated relative permeability in heterogeneous multiphase systems, *Adv. Water Res.*, *30*, 1144–1159.

Imhoff, P. T., P. Jaffe, and G. Pinder (1994), An experimental study of complete dissolution of a nonaqueous phase liquid in saturated porous media, *Water Resour. Res.*, *30*, 307–320.

Lemke, L. D., and L. Abriola (2006), Modeling dense nonaqueous phase liquid mass removal in nonuniform formation: Linking source zone architecture and system response, *Geosphere*, *2*(2), 74–82.

Maji, R., and E. Sudicky (2008), Influence of mass transfer characteristics for DNAPL source depletion and contaminant flux in a highly characterized glaciofluvial aquifer, *J. Contam. Hydrol.*, *102*, 105–119.

McClure, P., and B. Sleep (1996), Simulation of bioventing for soil and ground-water remediation, *J. Environ. Eng.*, *122*, 1003–1011.

Miller, C., M. M. Poirier-McNeill, and A. S. Mayer (1990), Dissolution of trapped nonaqueous phase liquids: Mass transfer characteristics, *Water Resour. Res.*, *26*, 2783–2796.

Morrow, N. R. (1970), Physics and thermodynamics of capillary action in porous media, *Industrial and Engineering Chemistry*, *62*, 32–56.

Nambi, I. M., and S. E. Powers (2000), NAPL dissolution in heterogeneous systems: An experimental investigation in a simple heterogeneous system, *J. Contam. Hydrol.*, *44*, 161–184.

Nambi, I. M., and S. E. Powers (2003), Mass transfer correlations for nonaqueous phase liquid dissolution from regions with high initial saturations, *Water Resour. Res.*, *39*(2), 1030, doi:10.1029/2001WR000667.

O'Carroll, D., and B. Sleep (2009), Role of NAPL thermal properties in the effectiveness of hot water flooding, *Transp. Porous Media*, *79*, 393–405.

O'Carroll, D., and B. E. Sleep (2007), Hot water flushing for immiscible displacement of a viscous NAPL, *J. Contam. Hydrol.*, *91*, 247–266.

Pfannkuch, H.-O. (1984), Determination of the contaminant source strength from mass exchange processes at the petroleum–ground-water interface in shallow aquifer systems, in *Proceedings of the NWWA/API Conference on Petroleum Hydrocarbons and Organic Chemicals in Ground Water—Prevention, Detection, and Restoration*, Houston, TX. Natl. Water Well Assoc., Worthington, OH, Nov. 1984, pp. 111–129.

Porter, M., D. Wildenschild, G. Grant, and J. I. Gerhard (2010), Measurement and prediction of the relationship between capillary pressure, saturation and interfacial area in a DNAPL-water-glass system, *Water Resour. Res.*, *46*, W08512, doi:10.1029/2009WR007786.

Powers, S. E., C. Loureiro, L. M. Abriola, and W. J. Weber Jr. (1991), Theoretical study of the significance of nonequilibrium dissolution of nonaqueous phase liquids in subsurface systems, *Water Resour. Res.*, *27*, 463–477.

Powers, S. E., L. M. Abriola, and W. J. Weber Jr. (1992), An experimental inverstigation of nonaqueous phase liquid dissolution in saturated subsurface systems: Steady state mass transfer rates, *Water Resour. Res.*, *28*, 2691–2705.

Powers, S. E., L. M. Abriola, J. S. Dunkin, and W. J. Weber Jr. (1994a), Phenomenological model for transient NAPL-water mass transfer processes, *J. Contam. Hydrol.*, *16*, 1–33.

Powers, S. E., L. M. Abriola, and W. Weber (1994b), An experimental investigation of NAPL dissolution in saturated subsurface systems: Transient mass transfer rates, *Water Resour. Res.*, *30*, 321–332.

Powers, S. E., I. M. Nambi, and G. W. Curry (1998), Non-aqueous phase liquid dissolution in heterogeneous systems: Mechanisms and a local equilibrium modeling approach, *Water Resour. Res.*, *34*, 3293–3302.

Rathfelder, K. M., L. M. Abriola, T. P. Taylor, and K. D. Pennell (2001), Surfactant enhanced recovery of tetrachloroethylene from a porous medium containing low permeability lenses: 2. Numerical simulation, *J. Contam. Hydrol.*, *48*, 351–374.

Saba, T., and T. Illangasekare (2000), Effect of groundwater flow dimensionality on mass transfer from entrapped nonaqueous phase liquid contaminants, *Water Resour. Res.*, *36*, 971–979.

Sale, T. C., and D. B. McWhorter (2001), Steady state mass transfer from single component dense nonaqueous phase liquids in uniform flow fields, *Water Resour. Res.*, *37*, 393–404.

Scroth, M. H., S. J. Ahearn, J. S. Selker, and J. D. Istok (1996), Characterization of miller-similar silica sands for laboratory hydrologic studies, *J. Soil Sci. Soc. Am.*, *60*, 1331–1339.

Seagren, E. A., B. E. Rittmann, and A. J. Valocchi (1999), A critical evaluation of the local equilibrium assumption in modeling NAPL-pool dissolution, *J. Contam. Hydrol.*, *39*, 109–135.

Sleep, B., and J. Sykes (1993), Compositional simulation of groundwater contamination by organic compounds: 1. Model development and verification, *Water Resour. Res.*, *29*, 1697–1708.

Sleep, B. E., L. Sehayek, and C. Chien (2000), A modeling and experimental study of light nonaqueous phase liquid (LNAPL) accumulation in wells and LNAPL recovery from wells, *Water Resour. Res.*, *36*, 3535–3545.

Suchomel, E. J., and K. D. Pennell (2006), Reductions in contaminant mass discharge following partial mass removal from DNAPL source zones, *Environ. Sci. Technol.*, *40*(19), 6110–6116, doi:10.1021/es060298e.

Unger, A. J. A., P. A. Forsyth, and E. A. Sudicky (1998), Influence of alternative dissolution models and subsurface heterogeneity on DNAPL disappearance times, *J. Contam. Hydrol.*, *30*(3–4), 217–242.

Yoon, H., C. Zhang, C. J. Werth, A. J. Valocchi, and A. G. Webb (2008), Three dimensional characterization of water flow in heterogeneous porous media using magnetic resonance imaging, *Water Resour. Res.*, *44*, W06405, doi:10.1029/2007WR006213.

Zhang, C., C. J. Werth, and A. G. Webb (2007), Characterization of NAPL source zone architecture and dissolution kinetics in heterogeneous porous media using magnetic resonance imaging, *Environ. Sci. Technol.*, *41*, 3672–3678.

Zhang, C., H. Yoon, C. J. Werth, A. J. Valocchi, N. B. Basu, and J. W. Jawitz (2008), Evaluation of simplified mass transfer models to simulate the impacts of source zone architecture on nonaqueous phase liquid dissolution in heterogeneous porous media, *J. Contam. Hydrol.*, *102*, 49–60.